Reports

Hidden Fermi Surface Nesting and Charge Density Wave Instability in Low-Dimensional Metals

M.-H. WHANGBO, E. CANADELL, P. FOURY, J.-P. POUGET

The concept of hidden Fermi surface nesting was introduced to explain the general observation that certain low-dimensional metals with several partially filled bands exhibit charge density wave (CDW) instabilities, although their individual Fermi surfaces do not reveal the observed nesting vectors. This concept was explored by considering the Fermi surfaces of the purple bronze AMo_6O_{17} (A = sodium or potassium) and then observing the CDW spatial fluctuations expected from its hidden nesting on the basis of diffuse x-ray scattering experiments. The concept of hidden Fermi surface nesting is essential for understanding the electronic instabilities of low-dimensional metals.

OWING TO MANY INTERESTING physical properties associated with their charge density wave (CDW) and spin density wave (SDW) phenomena, low-dimensional metallic compounds have been extensively studied (*1–6*). The normal metallic state of a low-dimensional metal is susceptible to a metal-to-insulator (MI) transition, such as a CDW or an SDW formation, when the temperature is lowered. Such an electronic instability of a low-dimensional metal occurs when its Fermi surface is nested (*5, 6*). A Fermi surface nesting is typically observed for a one-dimensional (1D) metal, for which the partially filled band is dispersive primarily along one direction. In certain cases, a CDW instability is observed for a two-dimensional (2D) metal with several Fermi surfaces, which, when analyzed separately, are 2D in nature and provide no apparent clue to the nesting responsible for the CDW. When all the Fermi surfaces are combined together, however, the resulting patterns can be decomposed into nested Fermi surfaces if the avoided crossings of these surfaces are neglected (*7, 8*). The nesting from such "hidden" Fermi surfaces, hereafter referred to as a hidden Fermi surface nesting (or, simply, a hidden nesting), causes a CDW formation that removes the nested portions of the combined Fermi surfaces. We explore here the concept of hidden nesting by investigating the Fermi surfaces of the purple bronze AMo_6O_{17} (A = Na, K) (*9*) and subsequently observing the CDW spatial fluctuations expected from its hidden nesting on the basis of diffuse x-ray scattering experiments.

As shown in Fig. 1A, a metal has at least one partially filled band. The energy $e(\mathbf{k})$ and the orbital $\phi(\mathbf{k})$ of a band level are a function of wave vector $\mathbf{k}$, normally taken from the first Brillouin zone (FBZ). For example, a rectangular 2D lattice with repeat distances a and b has the FBZ defined by the vectors $\mathbf{k} = (k_a, k_b)$ satisfying the conditions that $-\pi/a \leq k_a \leq \pi/a$ and $-\pi/b \leq k_b \leq \pi/b$. All the energy levels of a band are represented by the wave vectors of the FBZ. Thus, for a partially filled band, some wave vectors of the FBZ are associated with the occupied band levels and the remaining wave vectors with the unoccupied band levels. The Fermi surface of a partially filled band is the boundary surface separating the occupied wave vectors from the unoccupied wave vectors. Figure 1B illustrates the regions of the occupied and unoccupied wave vectors (shaded and unshaded, respectively) of a half-filled 1D band dispersive only along the $\Gamma \rightarrow X$ direction (that is, metallic along the a direction). The Fermi surface of this band consists of two parallel lines perpendicular to the $\Gamma \rightarrow X$ direction at $\pm \pi/2a$ (that is, $\pm k_f$) from Γ. Figure 1B shows that, when translated by a vector $\mathbf{q}$, the left-hand piece of the Fermi surface (that is, the vertical line at $-k_f$) is superposed to the right-hand piece of the Fermi surface. In general, when a piece of a given Fermi surface is superposed to another piece by a translational vector $\mathbf{q}$, the Fermi surface is said to be nested by the vector $\mathbf{q}$. For an ideal 1D surface such as the one in Fig. 1B, many different nesting vectors are possible. These vectors differ in their components along $\Gamma \rightarrow Y$, but their components along $\Gamma \rightarrow X$ are identical (that is, $2k_f$).

Under a perturbation H', an occupied band level $\phi(\mathbf{k})$ of a normal metallic state interacts with an unoccupied band level $\phi(\mathbf{k}')$ leading to new orbitals $\Psi(\mathbf{k}) \propto \phi(\mathbf{k}) + \lambda\,\phi(\mathbf{k}')$ and $\Psi(\mathbf{k}') \propto -\lambda\,\phi(\mathbf{k}) + \phi(\mathbf{k}')$, where λ is a mixing coefficient. Such an orbital mixing introduces a density wave in the new orbitals $\Psi(\mathbf{k})$ and $\Psi(\mathbf{k}')$, whose periodicity is described by $\cos(\mathbf{q} \cdot \mathbf{R})$, where $\mathbf{q} = \mathbf{k}' - \mathbf{k}$ and $\mathbf{R}$ is the vector defining the position of the lattice sites (*7, 10–12*). The electron density waves resulting from the orbitals $\Psi(\mathbf{k})$ and $\Psi(\mathbf{k}')$ are out of phase in that $\Psi(\mathbf{k})$ accumulates electron density where $\Psi(\mathbf{k}')$ depletes electron density. From sets of orbitals $\phi(\mathbf{k})$ and $\phi(\mathbf{k}')$ related by $\mathbf{q} = \mathbf{k}' - \mathbf{k}$, sets of new orbitals $\Psi(\mathbf{k})$ and $\Psi(\mathbf{k}')$ can be constructed. A CDW state is obtained when the orbitals $\Psi(\mathbf{k})$ are each doubly occupied, and an SDW state is derived when the orbitals $\Psi(\mathbf{k})$ and $\Psi(\mathbf{k}')$ are each singly occupied with up-spin and down-spin electrons, respectively. For a nested Fermi surface with vector $\mathbf{q}$, the orbitals $\phi(\mathbf{k})$ and $\phi(\mathbf{k}')$ related by $\mathbf{q} = \mathbf{k}' - \mathbf{k}$ are degenerate when $\mathbf{k}$ lies on the Fermi surface ($\mathbf{k}$ with the $\Gamma \rightarrow X$ component of $\pm k_f$, that is, $\mathbf{k}_f$), but nondegenerate otherwise (see Fig. 1B). In general, an interaction between two orbitals becomes strong as the energy difference between the two de-

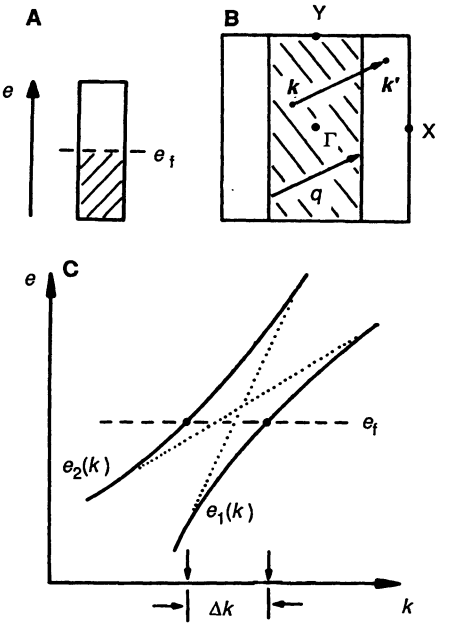

Fig. 1. (**A**) Schematic representation of a half-filled band. (**B**) Two-dimensional representation of the Fermi surface associated with a half-filled band dispersive along the $\Gamma \rightarrow X$ direction. The occupied and unoccupied wave vectors are found in the shaded and unshaded areas, respectively. $\Gamma = (0, 0)$; $X = (a^*/2, 0)$; $Y = (0, b^*/2)$; and $M = (a^*/2, b^*/2)$; where $a^* = 2\pi/a$ and $b^* = 2\pi/b$. (**C**) Schematic drawing of two band dispersion curves with an avoided crossing near the Fermi level.

M.-H. Whangbo, Department of Chemistry, North Carolina State University, Raleigh, NC 27695.
E. Canadell, Laboratorie de Chimie Théorique, Université de Paris–Sud, 91405 Orsay, France.
P. Foury and J.-P. Pouget, Laboratoire de Physique des Solides, Université de Paris–Sud, 91405 Orsay, France.

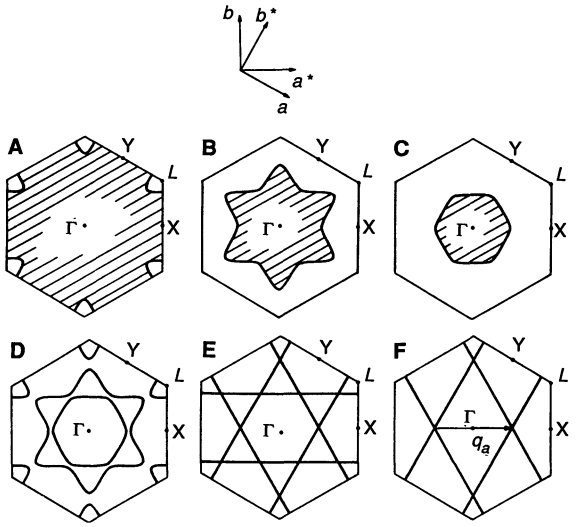

Fig. 2. Hidden nesting in the purple bronze KMo_6O_{17}. The calculated Fermi surfaces for the three partially filled *d*-block bands are shown in (**A**), (**B**), and (**C**), the combined Fermi surfaces in (**D**), and the hidden 1D Fermi surfaces in (**E**). Two sets of the hidden 1D surfaces are nested by a common vector q_a in (**F**). As shown in (A) to (F), the FBZ of a 2D trigonal lattice is given by a hexagon. Γ = (0, 0); X = ($a^*/2$, 0); Y = (0, $b^*/2$); and *L* = ($a^*/3$, $b^*/3$).

creases (*13*). If a Fermi surface is nested, the occupied and unoccupied band levels related by the nesting vector $\mathbf{q} = \mathbf{k}' - \mathbf{k}$ have very small or no energy difference for all the vectors $\mathbf{k}$ on or in the vicinity of the Fermi surface. Thus, a low-dimensional metal with a nested Fermi surface is susceptible toward a CDW or an SDW formation. The interaction between two orbitals associated with $\mathbf{k} = \mathbf{k}_f$ introduces an energy gap 2Δ at the Fermi level, where $\Delta = \langle\phi(\mathbf{k}_f)|H'|\phi(\mathbf{k}'_f)\rangle$, so that a CDW or an SDW formation removes the nested portions of the Fermi surface. The perturbation *H'* causing the orbital mixing is lattice vibration for CDW states and electron-electron repulsion for SDW states (*7, 10–12*). A CDW formation introduces an additional periodicity of electron density distribution into the lattice and hence gives rise to superlattice reflections in the x-ray or electron diffraction pattern below the CDW phase transition temperature T_p. At temperatures above T_p, a nested 1D Fermi surface leads to CDW fluctuations. The latter cause planar diffuse scattering and hence $2k_f$ diffuse lines between layers of main Bragg reflections in x-ray diffraction patterns (*14, 15*).

Analysis of Fermi surface nesting requires a special consideration for a low-dimensional metal with several partially filled bands. Figure 1C illustrates two band-dispersion curves with an avoided crossing in the vicinity of the Fermi level. When the extent of band hybridization increases, the separation Δk between the Fermi vectors becomes larger. In general, such avoided crossings in band-dispersion surfaces lead to avoided crossings in the corresponding Fermi surfaces. Therefore, a low-dimensional metal with several partially filled bands may give rise to apparently unnested Fermi surfaces, although their "intended" surfaces (that is, those expected in the absence of the avoided crossings) are all nested. In such a case, the nesting is "hidden" by the avoided crossings.

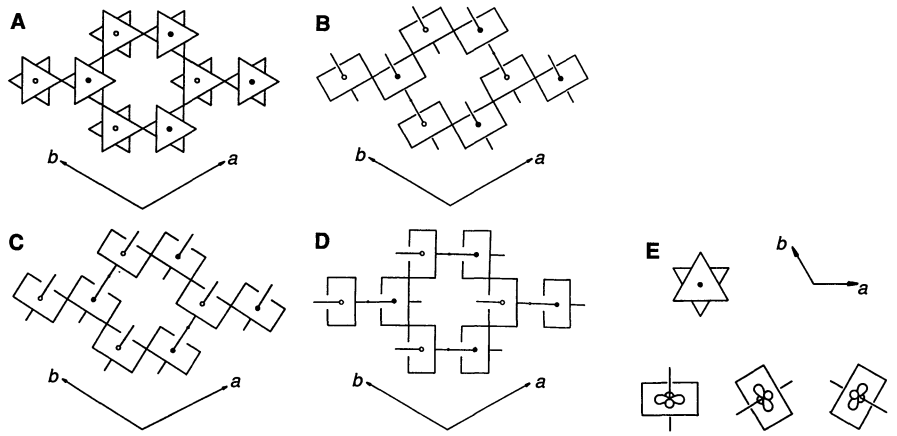

Fig. 3. Schematic views of the Mo_6O_9 trigonal layer present in the purple bronze AMo_6O_{17}. The projection view perpendicular to the layer is shown in (**A**). The Mo_2O_9 layer is constructed in terms of the Mo_2O_{10} zigzag chains running along the *a*, *b*, and (*a* + *b*) directions in (**B**), (**C**), and (**D**), respectively. Perspective views of the three t_{2g} orbitals of an MoO_6 octahedron in the Mo_2O_9 layer are shown in (**E**), where the *d* orbital–containing planes are aligned along the *a*, *b*, and (*a* + *b*) directions of the Mo_2O_9 layer.

To understand the CDW phenomenon of a low-dimensional metal with several partially filled bands, it is essential to search for a nesting in the intended, hidden Fermi surfaces. We now examine the concept of hidden nesting by taking the purple bronze AMo_6O_{17} (A = Na, K) as a prototype example. This bronze is a 2D metal and undergoes a CDW phase transition at 120 K (*16*). It remains 2D metallic below the CDW transition. Diffuse x-ray scattering and electron diffraction studies show the superlattice spots at $a^*/2$, $b^*/2$, and ($a^* - b^*$)/2 below 120 K (*17, 18*).

AMo_6O_{17} has three electrons per unit cell to fill its three lowest lying *d*-block bands, so that there are three partially filled *d*-block bands (*19*). The Fermi surfaces of the three bands are shown in Fig. 2, A, B, and C. These surfaces are all 2D in nature, and their individual partial nesting does not explain the observed CDW vectors. The three surfaces are combined in Fig. 2D, which, upon neglecting the avoided crossings, can be decomposed into three sets of nested 1D surfaces (Fig. 2E). The 1D Fermi surfaces are perpendicular to the *a*, *b*, or (*a* + *b*) direction of the trigonal lattice (*20*).

To a first approximation, therefore, the three partially filled bands of AMo_6O_{17} are derived from three 1D bands dispersive along the *a*, *b*, and (*a* + *b*) direct. This conclusion is consistent with the structural and electronic properties of this bronze. It consists of Mo–O layers with the composition Mo_6O_{17} separated by K^+ ions (*20*). According to the bond valence sum analysis of the Mo–O bonds, the *d* electrons of this bronze are contained in the inner Mo–O layer with composition Mo_2O_9 (*20*) made up of MoO_6 octahedra (see Fig. 3A). This layer is constructed from Mo_2O_{10} zigzag chains, running along the *a*, *b*, or (*a* + *b*) direction, by sharing their "axial" O atoms as shown in Fig. 3, B, C, and D (*19*). The partially filled bands of AMo_6O_{17} are made up of the t_{2g} orbitals of MoO_6 octahedra (*19*). The t_{2g} orbitals are contained in the planes of the chains (that is, those defined by the "equatorial" O atoms) running along the *a*, *b*, and (*a* + *b*) directions (Fig. 3E). Thus the t_{2g} orbitals are π orbitals along the intrachain directions but δ orbitals along the interchain directions (*19*), so that the t_{2g} orbitals of the Mo_2O_9 layer lead to three 1D bands dispersive along the *a*, *b*, and (*a* + *b*) directions. Because there are three electrons to fill these bands, each 1D band is half-filled.

Let us now consider the nature of the observed nesting vectors of AMo_6O_{17}. The superlattice spots at, for example, $a^*/2$ and $b^*/2$ show that the nesting vectors deviate from the chain directions. This finding can

be explained by the principle of maximum nesting: Given several different nesting possibilities, the nesting vector most likely to be observed is the one that maximizes the nested Fermi surface area because such a vector will maximize the electronic energy gain associated with CDW formation. Any two sets of the three 1D surfaces can be nested simultaneously by a single vector (Fig. 2E). This is illustrated in Fig. 2F. When the 1D bands are each half filled, it is straightforward to show that $q_a = a^*/2$ in Fig. 2F. The other two such nesting vectors of Fig. 2E are $q_b = b^*/2$ and $q_{a+b} = (a^* - b^*)/2$. The three vectors q_a, q_b, and q_{a+b} account for the superlattice spots observed for AMo_6O_{17} below 120 K (*17, 18*). The nesting in the real Fermi surfaces (Fig. 2D) is not so complete as in the hidden surfaces (Fig. 2E), so that some small pieces of Fermi surface (for example, small electron and hole pockets) may remain (especially in the avoided crossing regions) after the CDW phase transition. This would explain the semimetallic properties of AMo_6O_{17} observed below 120 K by galvanometric measurements (*21*). However, it is possible that the combined Fermi surface of a low-dimensional metal is removed completely, thereby leading to an MI transition, if the energy lowering resulting from a hidden nesting exceeds the energy required for the decoupling of band hybridization.

As far as the nesting is concerned, the electronic structure of AMo_6O_{17} is essentially represented by the three 1D bands. Then, like any 1D metallic system with CDW instability (*14, 15*), AMo_6O_{17} is expected to show 1D CDW fluctuations above 120 K. To confirm this prediction, we have performed diffuse x-ray scattering experiments on AMo_6O_{17} (A = Na, K) at room temperature with the monochromatic Laue scattering method (*15*), in which a fixed sample is placed in an incoming monochromatic x-ray beam (MoK_α, wavelength = 0.711 Å) and the x-ray diffuse scattering is collected on a photographic plate placed behind the sample. To obtain the principal information in the (a^*, b^*) reciprocal plane, the incoming beam was aligned approximately along the trigonal axis (that is, the c axis) of the sample.

Figure 4A shows an x-ray pattern obtained for KMo_6O_{17}. The trigonal symmetry of the diffraction patterns is clearly visible. There are two kinds of intense diffuse scattering passing through the main Bragg reflections (*18*). In addition, the x-ray pattern reveals a third kind of diffuse scattering in the form of faint diffuse lines often interrupted and situated midway between layers of the main Bragg reflections (indicated by long white arrows). This corresponds, in position and direction, to the diffuse scattering expected from the hidden nesting of KMo_6O_{17} (schematically presented in Fig. 4B). As expected, three sets of diffuse lines related by the trigonal symmetry are observed. They form hexagons around each main Bragg reflection (Fig. 4B). Some of the hexagons are shown by short white arrows in Fig. 4A. Although not shown, $NaMo_6O_{17}$ gives identical results. Consequently, the hidden nesting of the purple bronze AMo_6O_{17} is firmly established. Below 120 K, the diffuse lines of Fig. 4B condense into satellite reflections at $a^*/2$, $b^*/2$, and $(a^* - b^*)/2$, which are the cross-section points of the diffuse lines.

The concept of hidden nesting allows us to understand the CDW phenomenon of other low-dimension metals. For example, the Magnéli phases Mo_4O_{11} (*4*) and the monophosphate tungsten bronzes (MPTBs) (*22*) all have several partially filled bands (*8, 12, 23*). The combined Fermi surfaces of these bands can be decomposed into nested 2D and 1D surfaces. The nested 2D surfaces can be further decomposed into two sets of nested 1D surfaces. The observed CDW vectors of the Magnéli phases (*24*) and the MPTBs (*25*) are all accounted for in terms of those hidden nestings. Thus, the concept of hidden nesting is essential for understanding the electronic instabilities of low-dimensional metals with several partially filled bands.

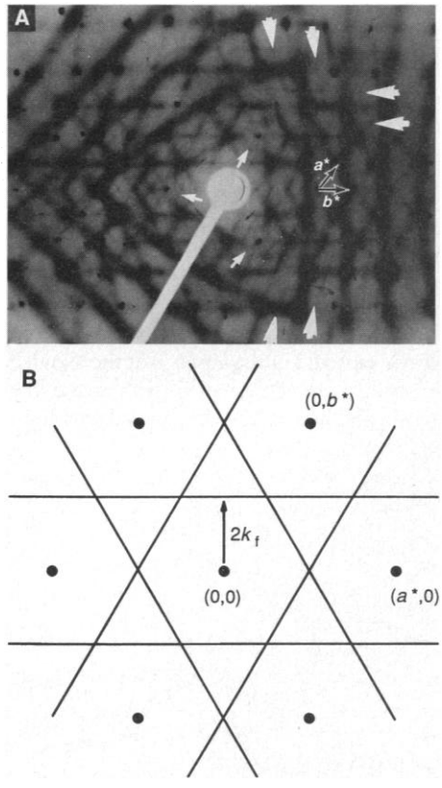

Fig. 4. (**A**) X-ray patterns obtained for KMo_6O_{17} at room temperature, where the trigonal reciprocal vectors **a*** and **b*** are indicated. Long white arrows point toward the $2k_f$ diffuse lines midway between layers of main Bragg reflections. Some hexagons delimited by the three sets of diffuse lines [outlined in (B)] are also shown by short white arrows. (**B**) Schematic representation of the diffuse lines expected from the hidden nesting of KMo_6O_{17} in the (a^*, b^*) plane, where the heavy dots refer to Bragg reflections.

REFERENCES AND NOTES

1. P. Monceau, Ed., *Electronic Properties of Inorganic Quasi-One-Dimensional Compounds* (Reidel, Dordrecht, The Netherlands, 1985), part III.
2. J. Rouxel, Ed., *Crystal Chemistry and Properties of Materials with Quasi-One-Dimensional Structures* (Reidel, Dordrecht, The Netherlands, 1986).
3. K. Motizuki, Ed., *Structural Phase Transitions in Layered Transition Metal Compounds* (Reidel, Dordrecht, The Netherlands, 1986).
4. C. Schlenker, Ed., *Low-Dimensional Electronic Properties of Molybdenum Bronzes and Oxides* (Reidel, Dordrecht, The Netherlands, 1989).
5. W. M. Lomer, *Proc. Phys. Soc. (London)* **80**, 489 (1962); A. W. Overhauser, *Phys. Rev.* **128**, 1437 (1962).
6. J. A. Wilson, F. J. DiSalvo, S. Mahajan, *Adv. Phys.* **24**, 117 (1975); F. J. DiSalvo, *Electron-Phonon Interactions and Phase Transitions* (Plenum, New York, 1977), p. 107.
7. M.-H. Whangbo and E. Canadell, *Acc. Chem. Res.* **22**, 375 (1989).
8. E. Canadell and M.-H. Whangbo, *Phys. Rev. B*, in press; E. Wang *et al.*, *ibid.* **39**, 12969 (1989).
9. The formulas for the sodium and potassium bronzes are traditionally written as $A_{0.9}Mo_6O_{17}$ (A = Na, K). However, there is evidence that the correct formulas should be AMo_6O_{17}. See A. Rotger *et al.*, *Synth. Metals*, in press.
10. M.-H. Whangbo, *J. Chem. Phys.* **73**, 3854 (1980); *ibid.* **75**, 4983 (1981).
11. _____, in *Electron Transfer in Biology and the Solid State: Inorganic Compounds with Unusual Properties*, M. K. Johnson *et al.*, Eds. (American Chemical Society, Washington, DC, 1990), p. 269.
12. E. Canadell and M.-H. Whangbo, *Chem. Rev.*, in press.
13. T. A. Albright, J. K. Burdett, M.-H. Whangbo, *Orbital Interactions in Chemistry* (Wiley, New York, 1985).
14. R. Moret and J.-P. Pouget, in (*2*), p. 87.
15. R. Comes and G. Shirane, in *Highly Conducting One-Dimensional Solids*, J. T. Devresse, R. P. Evrard, V. E. Van Doren, Eds. (Plenum, New York, 1979), p. 17.
16. C. Schlenker *et al.*, *Philos. Mag. B* **52**, 643 (1985); R. Buder *et al.*, *J. Phys. Lett.* **43**, L59 (1982).
17. J.-P. Pouget, in (*4*), p. 87.
18. C. Escribe-Filippini *et al.*, *Philos. Mag. B* **50**, 321 (1984).
19. M.-H. Whangbo, E. Canadell, C. Schlenker, *J. Am. Chem. Soc.* **109**, 6308 (1987).
20. H. Vincent *et al.*, *J. Solid State Chem.* **47**, 113 (1983).
21. C. Schlenker *et al.*, in (*4*), p. 159.
22. B. Raveau, *Proc. Indian Natl. Sci. Acad. Part A* **52**, 67 (1986).
23. E. Canadell, M.-H. Whangbo, C. Schlenker, C. Escribe-Filippini, *Inorg. Chem.* **28**, 1466 (1989).
24. H. Guyot *et al.*, *J. Phys. C* **18**, 4427 (1985).
25. P. Foury, J.-P. Pouget, E. Wang, M. Greenblatt, *Synth. Metals*, in press.

26. Part of this work, carried out at North Carolina State University, was supported by U.S. Department of Energy, Office of Basic Sciences, Division of Materials Sciences grant DE-FG05-86ER45259. Invaluable discussions with A. Rotger and C. Schlenker are acknowledged. The purple bronzes used in the x-ray study were provided by J. Marcus (LEPES-CNRS, Grenoble).

12 December 1990; accepted 24 January 1991